Mechanistic Investigation on Self-redox Decompositions of Cobalt−Hydroxide−Nitrate Compounds with Different Nitrate Anion Configurations in Interlayer Space

Rong Xu and Hua Chun Zeng*

Department of Chemical and Environmental Engineering, Faculty of Engineering, and Chemical and Process Engineering Center, National University of Singapore, 10 Kent Ridge Crescent, Singapore 119260

Received November 25, 2002. Revised Manuscript Received March 14, 2003

Self-redox decompositions of two cobalt−hydroxide−nitrates [$Co^{II}_{0.80}Co^{III}_{0.20}(OH)_{2.00}(NO_3)_{0.14}(CO_3)_{0.03}\cdot 0.77H_2O$ and $Co^{II}(OH)_{1.50}(NO_3)_{0.40}(CO_3)_{0.05}\cdot 0.05H_2O$] have been investigated with various analytical methods under an oxygen-free atmosphere. The investigated compounds all have a lamellar structure in which an oxidant layer (nitrate) and a reductant layer (Co^{2+}) are stacked in an alternate manner. In addition to the "molecular" level mixing of reagents, these compounds are purposely prepared with variations of reactant concentration and anion configuration in the interlayer space. It is found that redox decompositions within the compounds take place according to the following sequence: (i) decomposition of carbonate anions, (ii) dehydroxylation of brucite-like layers, and (iii) decomposition of nitrate anions, although actual reaction temperatures and gas-evolving patterns are different in the two cases. The nitrate decomposition can be ascribed to an attachment of nitrate anion to divalent cobalt of forming cobalt−oxides after the dehydroxylation. More complete decomposition has been observed for the compound that "stores" more redox reagents with direct contact in its lamellar structure, although the final decomposed products of both compounds are all in nanophase Co_3O_4 (12−15 nm; formed at 400 °C). Surface compositions of the studied samples have also been examined for the decompositions.

Introduction

Research on metal−hydroxide−salts has received considerable attention in recent years owing to interest in new applications. For example, applications of hydrotalcite-like compound based anionic clays have been extended from conventional areas, such as fabrications of catalysts, ceramics, anion adsorbents, medicine stabilizers, and ion exchangers,[1−3] to some newly emerging fields, such as organic−inorganic nanocomposites,[3−5] biomolecular−inorganic nanohybrids,[6,7] and precursors for nanostructured materials synthesis.[8−10]

In transition-metal hydroxides, cations (normally in divalent state $M^{II} = Mn^{2+}$, Fe^{2+}, Co^{2+}, Ni^{2+}, Cu^{2+}, Zn^{2+}, etc.) are located in the centers of oxygen octahedra formed by hydroxyl groups. The metal-containing octahedra then share their edges to form two-dimensional infinite sheets that are similar to the layered compound $Mg(OH)_2$ (brucite) with hexagonal symmetry.[1−3,11,12] The brucite-like sheets can stack upon one another via various chemical interactions between the sheets along the *c* axis. Intercalation of anions to the inter-brucite-like-sheet space (interlayer space) can further take place, which will lead to the formation of metal−hydroxide−salts. When some of the hydroxyl groups in brucite-like sheets are missing, substitution of anions (e.g., nitrate ions) occurs, owing to attractive interaction between the metal cations and anions.[13] On the other hand, when some of the divalent cations are replaced by the trivalent ones (e.g., $M^{III} = Al^{3+}$, Ga^{3+}, Cr^{3+}, Mn^{3+}, Fe^{3+}, Co^{3+}, etc.), inorganic, organic, and even biomolecular anions will be intercalated into the interlayer space to compensate extra charges introduced by the trivalent cations. This type of metal−hydroxide−salt is also called hydrotalcite-like compound (HTlc).[1−3] The basis of this intercalation is electrostatic, which results in a lamellar structure with a sequential charge stacking of positive-then-negative along the *c*-axis, as found in natural hydrotalcite compound $Mg_6Al_2(OH)_{16}CO_3\cdot 4H_2O$.[14,15]

* To whom correspondence should be addressed. E-mail: chezhc@nus.edu.sg.

(1) Cavani, F.; Trifiro, F.; Vaccari, A. *Catal. Today* **1991**, *11*, 173, and references therein.
(2) Vaccari, A. *Catal. Today* **1998**, *41*, 53, and references therein.
(3) Rives, V.; Ulibarri, M. A. *Coord. Chem. Rev.* **1999**, *181*, 61, and references therein.
(4) Cai, H.; Hillier, A. C.; Franklin, K. R.; Nunn, C. C.; Ward, M. D. *Science* **1994**, *266*, 1551.
(5) Leroux, F.; Besse, J. P. *Chem. Mater.* **2001**, *13*, 3507.
(6) Choy, J. H.; Kwak, S. Y.; Park, J. S.; Jeong, Y. J.; Portier, J. *J. Am. Chem. Soc.* **1999**, *121*, 1399.
(7) Choy, J. H.; Kwak, S. Y.; Jeong, Y. J.; Park, J. S. *Angew. Chem., Int. Ed.* **2000**, *39*, 4042.
(8) Xu, Z. P.; Zeng, H. C. *J. Phys. Chem. B* **2000**, *104*, 10206.
(9) Xu, Z. P.; Xu, R.; Zeng, H. C. *Nano Lett.* **2001**, *1*, 703.
(10) Sampanthar, J. T.; Zeng, H. C. *Chem. Mater.* **2001**, *13*, 4722.
(11) Brindley, G. W.; Kikkawa, S. *Am. Mineral.* **1979**, *64*, 836.
(12) (a) Xu, Z. P.; Zeng, H. C. *Chem. Mater.* **1999**, *11*, 67. (b) Xu, Z. P.; Zeng, H. C. *J. Phys. Chem. B* **2001**, *105*, 1743.
(13) Poul, L.; Jouini, N.; Fiévet, F. *Chem. Mater.* **2000**, *12*, 3123.
(14) Allmann, R. *Acta Crystallogr.* **1968**, *B24*, 972.
(15) Taylor, H. F. W. *Miner. Magn.* **1969**, *37*, 338.

10.1021/cm021732o CCC: $25.00
Published on Web 04/10/2003

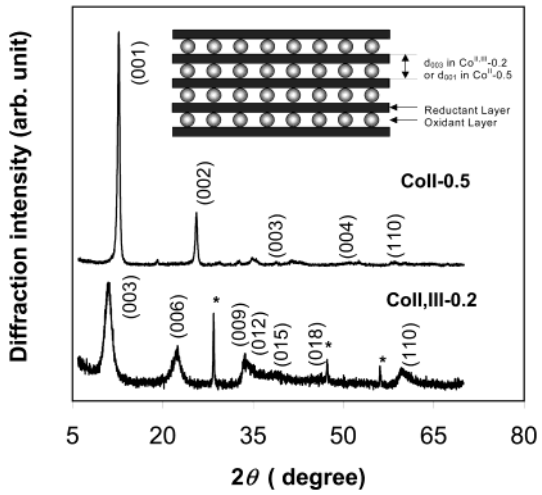

Figure 1. XRD patterns of two cobalt−hydroxide−nitrate compounds $Co^{II,III}$-0.2 and Co^{II}-0.5 investigated in this work. Reflections of polycrystalline silicon (internal standard) are indicated with an asterisk. Insert indicates an alternate arrangement of oxidant and reductant in the two compounds and inter-brucite-like-sheet-distance assignments under two different crystal symmetries.

In view of their special structural and electronic features, tailor-making these metal−hydroxides−salts opens new avenues for synthesis of nanostructured materials. For example, anions of oxometalates (from low to high nuclearity) and complexes of macrocyclic ligands and polymeric anions have also been intercalated into the interlayer space, generating inorganic or organic nanocomposites.[3,5,16] Furthermore, large-sized biomolecular anions (up to a few nm) such as nucleoside monophosphates and deoxyribonucleic acid (DNA) have been intercalated into the interlayer space of $Mg_{0.68}Al_{0.32}(OH)_2(NO_3)_{0.32}\cdot 1.2H_2O$ via anion exchange.[6,7] It is believed that the brucite-like sheets can protect the intercalated bio- or drug anions from degradation, and the charge neutralization can enhance the transfer of hydrotalcite hybrids into mammalian cells through endocytosic means.[6,7] Recently, we treated the intercalated anions such as organic and polymeric anions as starting materials (reactants) in a "nanoscale reactor" constructed by two adjacent brucite-like sheets for solid-state synthesis of nanocarbons.[8,9] Upon heating, the brucite-like sheets of HTlcs decompose into catalytically active metal−oxides, which will then accelerate carbonization reactions of the intercalated anions.[8,9] Apart from the above new applications, thermal decomposition of HTlcs can also be utilized as a common means for the fabrication of nanostructured metal−oxides and composite derivatives.[10,17] In this regard, chemical reactivity between the intercalated anions and metal cations in the brucite-like sheets has to be addressed in detail with the aim at a better design of precursor compounds.

Regarding the chemical reactions, one of the most interesting reactant combinations is the alternate stacking of oxidation agents and reducing agents within the lamellar structures of these compounds (see Figure 1), noting that these reactants are mixed at the molecular level prior to redox decomposition. This special material arrangement is raised because the cations in the divalent state may further lose electrons when they encounter oxidants during the decomposition. Very recently, we examined oxidation−reduction capacity of cobalt-containing HTlcs and its effect on the final morphologies and surface textures of decomposed products—Co_3O_4 nanoparticles.[18] More specifically, flat-lying oxidative anion such as nitrate and non-oxidative anions such as carbonate in the interlayer space, and their chemical reactivity toward divalent cobalt during the decomposition reactions, have been comparatively studied. In this article, as a first attempt, we will carry out a comparative investigation on the dynamic aspects of intracompound redox reactions of two cobalt−hydroxide−nitrates with different nitrate anion configurations associated to the divalent metal cations.

Experimental Section

Materials Preparation. Two cobalt−hydroxide−nitrate compounds were prepared using two different precipitation methods. The first sample, named $Co^{II,III}$-0.2 (0.2 denotes total charge carried by intercalated anions), was synthesized by adding 20.0 mL of cobalt nitrate solution at 1.0 M ($Co(NO_3)_2\cdot 6H_2O$, >99%, Merck) into 100.0 mL of 0.5 M ammoniacal solution under magnetic stirring in a three-necked round-bottom flask within 4 min. The addition and precipitation were carried out with magnetic stirring and a purified air stream (Soxal, $O_2 = 21 \pm 1\%$, $H_2O < 2$ vpm (volume per million), and hydrocarbons < 5 vpm) bubbling through the solution at a rate of 40 mL min^{-1}. The stirring and ambient control were continued during an aging process of the precipitate for 24 h, after which the precipitate was filtered and washed thoroughly with deionized water, followed by drying in a vacuum desiccator at room temperature overnight. The second sample, named Co^{II}-0.5 (0.5 denotes total charge carried by intercalated anions), was prepared by adding 20.0 mL of cobalt nitrate solution at 1.0 M into the same round-bottom flask containing 100.0 mL of sodium hydroxide solution at 0.3 M (NaOH, >98%, Fluka) and 110.0 g of sodium nitrate ($NaNO_3$, >99%, Nacalai Tesque) within 1 min. During the metal addition, the temperature of the solution was maintained at 95 °C under vigorous stirring. The precipitate (in the mother liquor) was aged at atmospheric pressure with continued stirring at 95 °C for another 3 h. After aging, the temperature of the final mixture was brought to room temperature and the resultant precipitate was processed with the same treatments as those for the first sample.

To understand the thermal behavior of the two samples during their decompositions, 20.0−21.0 mg of the as-prepared samples was loaded into a platinum crucible and heated in a thermogravimetric analysis apparatus (TGA, Model-2050, Bio-Rad) up to 220, 300, and 400 °C, respectively, and then cooled to room temperature. The ramp rate was set at 10 °C min^{-1} and a nitrogen stream (gas flow rate = 100 mL min^{-1}) was used to ensure an inert environment for the self-redox decompositions.

Materials Characterization. Crystallographic information of the two samples was investigated by powder X-ray diffraction (XRD). Diffraction patterns of intensity versus 2θ were recorded in a Shimadzu X-ray diffractometer (Model 6000) with Cu Kα radiation ($\lambda = 1.5406$ Å) at a scanning speed of 1° min^{-1}. The interlayer spacing of the resultant hydroxide−nitrate compounds was determined from the diffraction peak positions/patterns with structural analysis software. Particle sizes of the heated samples were estimated from full-width at half-maximums (fwhm's) of certain intense XRD diffraction

(16) Millange, F.; Walton, R. I.; Lei, L.; O'Hare, D. *Chem. Mater.* **2000**, *12*, 1990.
(17) Xu; Z. P.; Zeng, H. C. *Chem. Mater.* **2001**, *13*, 4564.
(18) Xu, Z. P.; Zeng, H. C. *Chem. Mater.* **2000**, *12*, 3459.

Table 1. Results of Compositional Analysis and Structural Analysis

sample	N%[a]	C%[a]	Co%[b]	H_2O%[c]	chemical formula
$Co^{II,III}$-0.2	1.71	0.25	50.2	10.0	$Co^{II}_{0.80}Co^{III}_{0.20}(OH)_{2.00}(NO_3)_{0.14}(CO_3)_{0.03}\cdot 0.77H_2O$
Co^{II}-0.5	4.99	0.48	50.8	0.7	$Co^{II}(OH)_{1.50}(NO_3)_{0.40}(CO_3)_{0.05}\cdot 0.05H_2O$

sample	phase	crystallite size	*d*-spacing	lattice parameter
$Co^{II,III}$-0.2	rhombohedral	7.0 nm[d] (15.5 nm)[e]	$d_{003} = 8.05$ Å $d_{006} = 4.01$ Å	$c = 24.11$ Å $a = 3.10$ Å
Co^{II}-0.5	hexagonal	19.0 nm[d] (12.3 nm)[e]	$d_{001} = 6.98$ Å $d_{002} = 3.48$ Å	$c = 6.97$ Å $a = 3.19$ Å

sample	calculated weight loss[f]	expt weight loss[g]
$Co^{II}_{0.80}Co^{III}_{0.20}(OH)_{2.00}(NO_3)_{0.14}(CO_3)_{0.03}\cdot 0.77H_2O$	31.6%	26.9%
$Co^{II}(OH)_{1.50}(NO_3)_{0.40}(CO_3)_{0.05}\cdot 0.05H_2O$	29.1%	30.7%

[a] Elemental wt % in sample determined from CHN analysis. [b] Metal wt % in sample determined from TGA analysis on the basis of final product Co_3O_4 at 600 °C in air. [c] Water wt % in sample measured from TGA analysis using the weight loss data before 150°C; [d] Dimensions of as-prepared crystallites in the *c* axis were calculated from fwhm's of (003) and (001) reflections for $Co^{II,III}$-0.2 and Co^{II}-0.5, respectively. [e] Crystallite sizes of cobalt spinel were determined from fwhm's of the (311) peak (Figure 7). [f] Theoretical weight loss according to final oxide products of Co_3O_4. [g] Experimental weight losses at 600 °C in nitrogen (TGA result; Figure 5).

peaks using Scherrer's method.[19] Chemical bonding information on metal−oxygen, metal−anions, and hydroxyl were studied with Fourier transform infrared spectroscopy (FTIR; Shimadzu Model-8101) using the potassium bromide (KBr) pellet technique and NaCl windows with Nujol mulls, respectively. Each FTIR spectrum was collected after 100 scans with a resolution of 2 cm^{-1} from 400 to 4000 cm^{-1}.

Elemental analysis for nitrogen and carbon contents in the prepared compounds was carried out with a Perkin-Elmer 2400 CHN analyzer. The cobalt content in each hydroxide−nitrate compound was measured by TGA on the basis of the final decomposed product Co_3O_4 at 600 °C in an air atmosphere. In particular, the content of trivalent cobalt in the $Co^{II,III}$-0.2 sample had been determined by a redox reaction, as detailed in our previous investigation.[18]

TGA study was conducted to investigate the thermal processes of the samples. Around 12 mg of each sample was heated at a rate of 10 °C min^{-1} over 24−600 °C in a nitrogen stream flowing at 100 mL min^{-1}. In combined TGA-FTIR measurements (TGA 2050, TA Instruments and FTIR, Bio-Rad), gases evolved from the sample heated with TGA were introduced into a measurement cell by carried gas (N_2 at a rate of 100 mL min^{-1}), and then a series of FTIR spectra were recorded every 4 s. To monitor the infrared absorption changes versus scanning time, that is, versus the temperature of TGA, the Gram-Schmidt reconstruction technique was used to construct the chromatogram from the collected set of interferograms.[20,21] In this work, the IR chromatograms of H_2O (3850−3857 cm^{-1}), CO_2 (2356−2380 cm^{-1}), and NO_2 (2915−2927 cm^{-1}) were thus prepared, and they were taken as dynamic measures of relative concentration of the evolved gaseous species versus time (or temperature) upon the decompositions of the two compounds.

X-ray photoelectron spectroscopy (XPS) investigation was carried out in an AXIS-Hsi spectrometer (Kratos Analytical) using a monochromated Al Kα X-ray source (1486.6 eV). The XPS spectra of studied elements were measured with the constant analyzer pass energy of 20.0 eV. All binding energies (BE) were referred to the C 1s peak (BE = 284.7 eV) arising from adventitious hydrocarbon.[9,10] Prior to the spectrum deconvolution, X-ray satellites and inelastic background (Shirley-type) were subtracted for all spectra. The full-width at half-maximum (fwhm) within the same core level of the elements was set to the same for all components. The atomic ratio was estimated by assuming the integrated baseline and the homogeneous surface layer and using Perkin-Elmer atomic sensitivity factors.

Results and Discussion

Structural and Chemical Analysis. Figure 1 displays the XRD patterns of $Co^{II,III}$-0.2 and Co^{II}-0.5 samples. The pattern of $Co^{II,III}$-0.2 exhibits broad symmetric peaks of (003) and (006) reflections of the hydrotalcite-like phases. The rest of the reflections are all broader and less symmetrical, indicating some turbostratic features related to stacking faults. The average inter-brucite-like sheet distance is 8.04 Å (=*c*/3), which is in the normal range of HTlcs with interlayer anions NO_3^- lying flat in the interlayer space. Chemical analysis (Table 1) confirms that this sample indeed has both +2 and +3 oxidation states for cobalt cations.[18] Compared to $Co^{II,III}$-0.2, the Co^{II}-0.5 sample shows a much sharper diffraction pattern for the peaks with lower 2θ values, which is identical to the literature data for cobalt−hydroxide−nitrate with a similar composition.[22] In this compound, cobalt ions are entirely in the divalent state and interlayer nitrate anions have been proposed to stand vertically.[23] A general chemical formula can be written as $M(OH)_{1.5}(NO_3)_{0.5}$ (M = Cu, Co, and Ni) for this type of divalent transition-metal−hydroxide−nitrates (involving a modification of the hydroxyl sublattice),[24,25] noting that various combinations with these metal ions are still possible in view of a small variation in their ionic radii.[22] According to the reported literature for $Cu(OH)_{1.5}(NO_3)_{0.5}$ and other α-type Co^{II}−hydroxides, reflection peaks of our Co^{II}-0.5 sample are also indexed with the hexagonal symmetry,[16,24,25] which has the same hydroxyl group stacking as in the case of brucite $Mg(OH)_2$.[23] The inter-brucite-like sheet distance is 6.98 Å (*c*) in Co^{II}-0.5.

(19) Cheetham, A. K.; Day, P. *Solid-State Chemistry: Techniques*; Clarendon Press: Oxford, 1987; p 79.
(20) Griffiths; P. R.; de Haseth, J. A. *Fourier Transform Infrared Spectrometry, Chemical Analysis*; Wiley-Interscience: New York, 1986; Vol. 83.
(21) Akinade, K. A.; Campbell, R. M.; Compton, D. A. C. *J. Mater. Sci.* **1994**, *29*, 3802.
(22) Zotov, N.; Petrov, K.; Dimitrova-Pankova, M. *J. Phys. Chem. Solids* **1990**, *51*, 1199.
(23) Effenberger, H. *Kristallographie* **1983**, *165*, 127.
(24) Rajamathi, M.; Kamath, P. V.; Seshadri, R. *Mater. Res. Bull.* **2000**, *35*, 271.
(25) Rajamathi, M.; Thomas, G. S.; Kamath, P. V. *Proc. Indian Acad. Sci. (Chem. Sci.)* **2001**, *113*, 671.

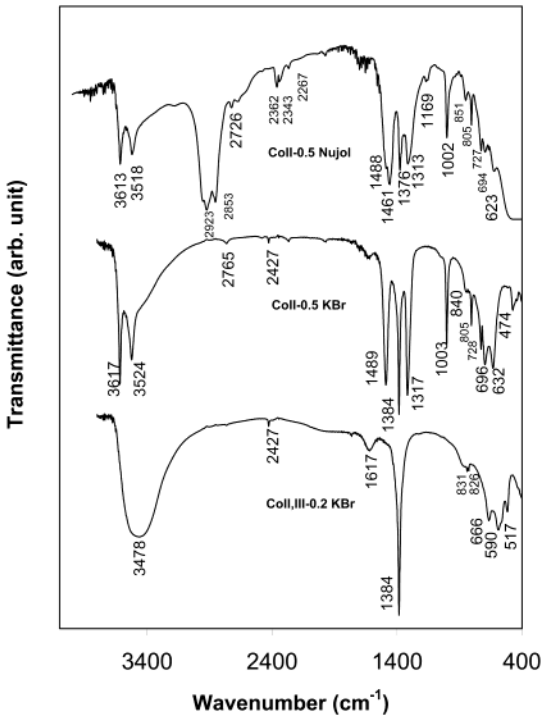

Figure 2. FTIR spectra of as-prepared cobalt−hydroxide−nitrate compounds $Co^{II,III}$-0.2 and Co^{II}-0.5 using KBr pellet and Nujol mull techniques.

Compared to that in $Co^{II,III}$-0.2, nitrate anion content in Co^{II}-0.5 is significantly higher, due to substoichiometric alkaline ($OH^-/Co^{2+} = 1.5$, instead of 2.0) and a huge amount of nitrate ions present (110 g of $NaNO_3$) in the initial solution.

Configurations of Nitrate Anions in Interlayer Space. In Figure 2, two different nitrate configurations in the interlayer space are evidenced by the observed IR active modes of the anion (the majority anions intercalated; Table 1). For the hydrotalcite-like compound $Co^{II,III}$-0.2, in particular, the intercalated anions are exclusively located in highly symmetrical sites with D_{3h} vibrational modes. The sharp peak at 1384 cm^{-1} is due to the ν_3 (E′) mode of D_{3h}, while a weak peak at 831 cm^{-1} (and 826 cm^{-1} also) is assigned to ν_2 (A″2) mode of the same symmetry.[22,26] Although it has been known that carbonate anions also adopt D_{3h} symmetry in interlayer space,[18] their ν_3 (1365 cm^{-1}, as a shoulder next to the 1384-cm^{-1} main peak) and ν_2 (870 cm^{-1}) modes are barely observed because of their low concentration.[22,26]

The implication of D_{3h} symmetry is that oxygen atoms of nitrate anions have the same interlayer positions as carbonate anions in natural hydrotalcite compound[14,15] in which every oxygen atom of a carbonate anion is aligned approximately with two hydroxyl groups above and below along the same vertical line via hydrogen bonding. As illustrated in Figure 3, stacking of hexagonally packed hydroxyl groups, metal cations, and interlayer anions in the hydrotalcite-like structure follows the sequence of B(A)C−C−C(B)A−A−A(C)B−B−B(A)C.[27,28] Taking our FTIR results into consideration, model I depicts the normal positions of nitrate anions in the interlayer space of $Co^{II,III}$-hydrotalcite-like compounds. In view of some turbostratic features in the XRD pattern of the $Co^{II,III}$-0.2 sample, model II is also proposed to explain our FTIR observation that the ν_2 mode (A″2) of this anion is in fact split into two components at 831 and 826 cm^{-1}, respectively. The nitrate anions in this model could still maintain their D_{3h} symmetry even when the random layer stacking occurs, yet clearly give a different local environment (compared to that in model I) for this out-of-plane bending vibration.[29] For example, when some of the hydroxyl groups adopt the same stacking sequence as that in the brucite structure (will be addressed shortly), the oxygen atoms of nitrate anions in model II will be bonded vertically to their immediate upper brucite-like-layer via hydrogen bonding. In this regard, a large broad absorption band centered at 3478 cm^{-1} is indeed observed, which is commonly attributed to hydrogen-bonded O−H stretching of OH in brucite-like-sheets and H_2O in interlayer space, noting that water bending mode is also found at 1617 cm^{-1}.[1−3]

The FTIR spectrum of Co^{II}-0.5 is quite different from that of $Co^{II,III}$-0.2 in several respects. First, vibrational modes of nitrate anion that belong to a lower site symmetry C_{2v} have been observed. According to literature data,[22,29,30] three strong and sharp peaks at 1489, 1317, and 1003 cm^{-1} can be assigned respectively to ν_5, ν_1, and ν_2 in C_{2v} symmetry.[26] The splitting of the degenerate E′ (ν_3 mode; D_{3h}) to give ν_5 and ν_1 modes is characteristic of bi- and monodentate NO_3 groups attaching to a metal cation (M−ONO_2).[22] IR peaks at around 805 and 696 cm^{-1} are assigned to ν_6 and ν_3 modes that correspond to out-of-plane and in-plane −ONO_2 vibrations.[22] The metal−hydroxyl (M−OH) and metal−oxygen (M−O) vibrations in sample Co^{II}-0.5 are also different. Absorption bands at around 632 and 474 cm^{-1} can be attributed to δ(M−OH) and ν(M−O), respectively, in this cobalt−hydroxide−nitrate,[22] noting that these bands have different wavenumbers in the hydrotalcite-like compound $Co^{II,III}$-0.2. Nonetheless, there have been concerns that KBr pellet may enhance the intensities of D_{3h} vibration bands of free nitrate anions due to a possible exchange reaction between nitrate anions from the sample and bromide ions from the KBr matrix.[22,26] To justify the detections of D_{3h} vibrational modes, Nujol mulls were also used in our FTIR measurements for the Co^{II}-0.5 sample (Figure 2). As can be seen, the ionic exchange reaction is not appreciable judging from relative intensities of nitrate characteristic bands/peaks measured by the latter method (1376 cm^{-1}, D_{3h} (Nujol, Figure 2); the shift from 1384 cm^{-1} is due to the different medium used). Therefore, nitrate anions with both D_{3h} and C_{2v} absorptions are indeed present in the Co^{II}-0.5 sample, which leads us to propose another new structural model (model II) in Figure 4 in addition to the known structure (model I) for this compound.[23−25] Starting from a vacant site of hydroxyl ion, a nitrate anion can have two adsorption configurations. The first one, which has been commonly known in the bound

(26) Ehlsissen, K. T.; Delahaye-Vidal, A.; Genin, P.; Figlarz, M.; Willmann, P. *J. Mater. Chem*. **1993**, *3*, 883.
(27) Allmann, R. *Chimia* **1970**, *24*, 99.
(28) Bellotto, M.; Rebours, B.; Clause, O.; Lynch, J.; Bazin, D.; Elkaim, E. *J. Phys. Chem*. **1996**, *100*, 8535.
(29) Gaddsden, J. A. *Infrared Spectra of Minerals and Related Inorganic Compounds*; Butterworth: London, 1975; p 22.
(30) Delahaye-Vidal, A.; Ehlsissen, K. T.; Genin, P.; Figlarz, M. *Eur. J. Solid State Inorg. Chem*. **1994**, *31*, 823.

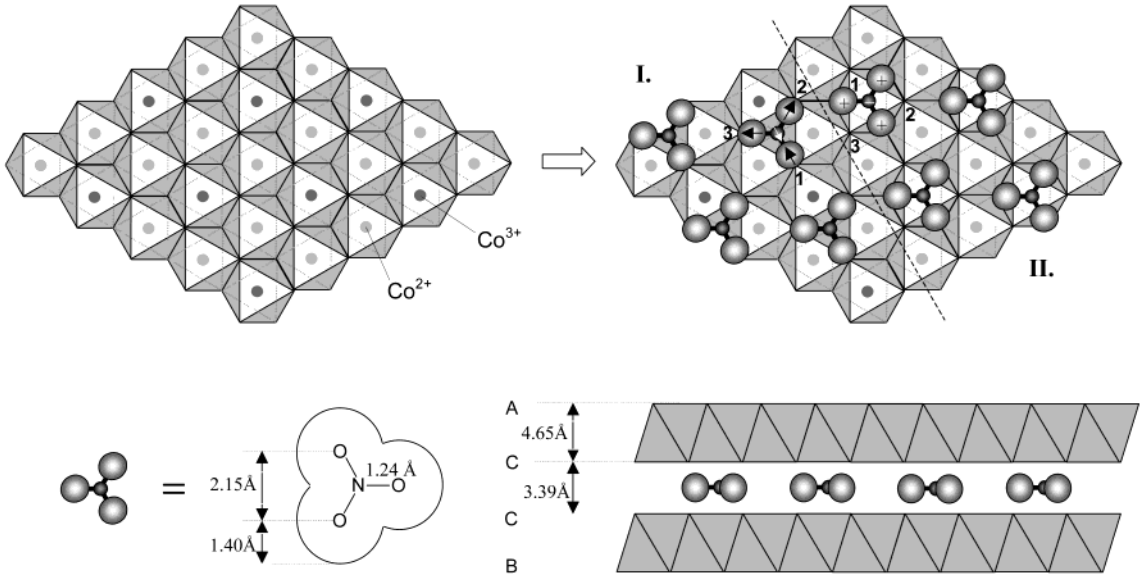

Figure 3. Nitrate anion configurations in interlayer space for a Co−hydrotalcite-like compound with one-third of the total cobalt cations in the trivalent oxidation state. In model I, every oxygen atom has two hydroxyl groups respectively from two adjacent brucite-like layers (above and below, marked with 1, 2, and 3). In model II, oxygen atoms are not connected directly to hydroxyl groups (marked with 1, 2, and 3) from the two adjacent brucite-like layers in the normal HT stacking sequence, but they may be connected to hydroxyl groups directly when a turbostratic stacking occurs in the upper layer. Arrows indicate the vibrational directions of atoms in asymmetric stretch mode (ν_3), while positive and negative signs show the out-of-plane bending mode (ν_2).

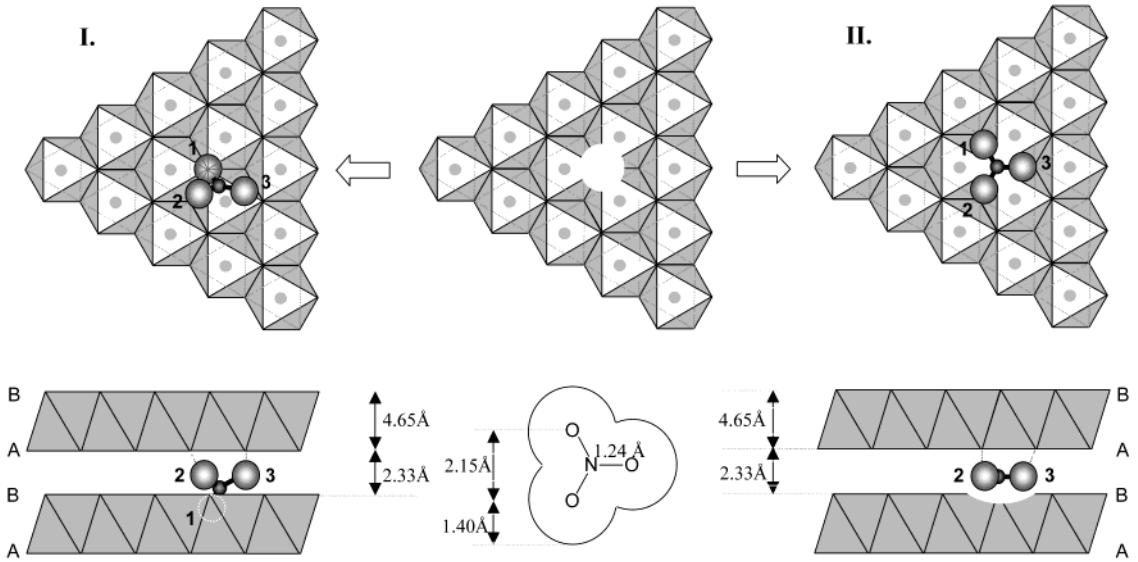

Figure 4. Nitrate anion configurations in interlayer space for a Co−hydroxide−nitrate compound in which all cobalt cations are in the divalent oxidation state. Starting from a hydroxyl vacancy, on one hand, a nitrate anion can be incorporated into the brucite-like plane through one of its three oxygen atoms (C_{2v}; model I), which leads to a modification of the hydroxyl sublattice. On the other hand, a nitrate anion could directly attach to the same vacancy with a D_{3h} site symmetry (model II).

state C_{2v},[23−25] involves a modification of the hydroxyl sublattice in the brucite-like sheets, as one of the oxygen atoms (atom 1) of anion is directly inserted into the basal plane in replacing a hydroxyl ion. The remaining two oxygen atoms in interlayer space are bound to one (atom 2; with one short H bond) and two (atom 3; with two longer H bonds) nearest hydroxyl groups via hydrogen bonding, respectively, in the brucite-like sheet on top of them. The second model takes the observed D_{3h} absorption modes into account, which allows all three oxygen atoms to attach equally to the three hydroxyl groups above, noting that a highly symmetrical environment for nitrate ions can still be maintained in this model even after they are sandwiched with another brucite-like sheet above.

One major difference between $Co^{II,III}$-0.2 and Co^{II}-0.5 is the content of water (Table 1 and water bands at 1617 cm^{-1}). Due to low water content and different nitrate configurations in Co^{II}-0.5, the O−H stretching band in this sample is better resolved. In particular, the peaks at 3617 and 3524 cm^{-1} can be assigned to two hydrogen-bonding modes of ν(O−H···O)′ and ν(O−H···O)″, respectively,[22] although a similar O−H band shape to that of $Co^{II,III}$-0.2 can still be recognized in the lower wavenumber region.

Self-redox Decomposition of Intercalated Nitrate Anions. In the TGA curves of $Co^{II,III}$-0.2 in Figure 5, three temperatures at around 65, 108, and 151 °C can be attributed respectively to physically adsorbed water on the surface, water trapped in intercrystallite

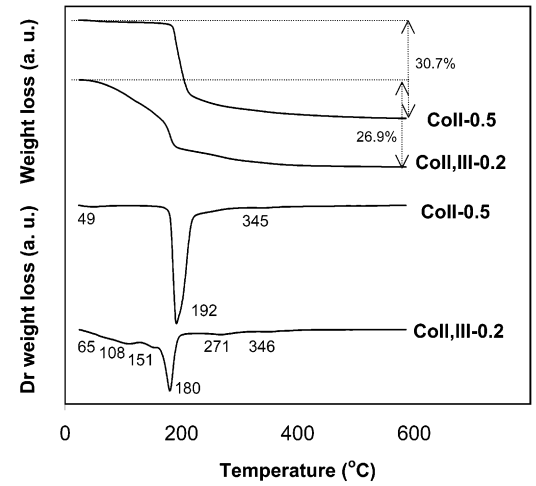

Figure 5. TGA and DTG scans for as-prepared $Co^{II,III}$-0.2 and Co^{II}-0.5 compounds heated in a nitrogen atmosphere.

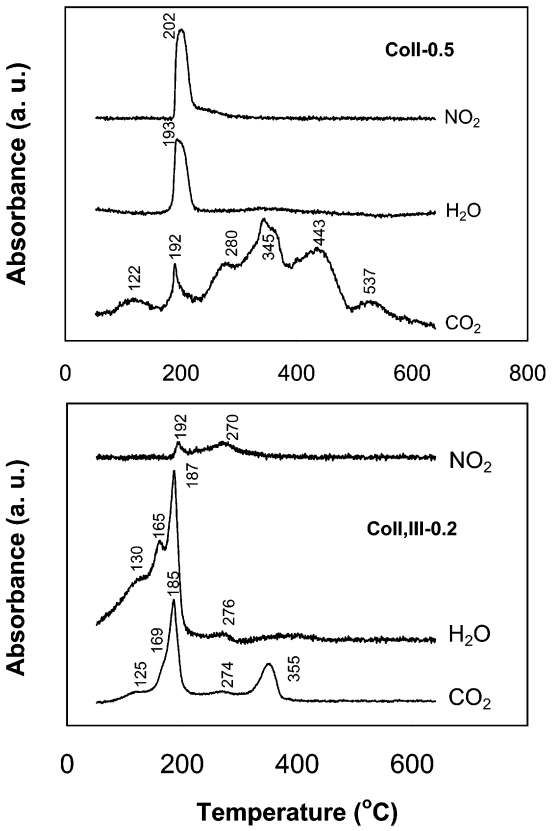

Figure 6. Integrated absorbances of evolved gases NO_2, H_2O, and CO_2 versus heating temperature in the combined TGA-FTIR measurements for the samples of (a) $Co^{II,III}$-0.2 and (b) Co^{II}-0.5.

pores,[31] and intercalated water in the interlayer space.[1−3] Consistent with this, the chromatogram of H_2O for the same sample also shows the similar water-releasing pattern, as displayed in Figure 6. At 180 °C, the major decomposition of the $Co^{II,III}$-0.2 compound occurs, which is characterized with a collapse of hydrotalcite-like structure and a release of decomposed gaseous products. The thermal sequence of $Co^{II,III}$-0.2 over this temperature range can be further differentiated: (i) decomposition of carbonate anions (185 °C); (ii) dehydroxylation of brucite-like layers (187 °C); and (iii) decomposition of nitrate anions (192 °C).

Co^{II}-0.5 shows only a very small weight loss of surface desorption and interlayer dehydration of water molecules prior to the major decompositions. The abrupt weight loss for this sample peaks at 192 °C (Figure 5), which can also be differentiated into three thermal events: (i) decomposition of carbonate anions (192 °C); (ii) dehydroxylation of brucite-like layers (193 °C); and (iii) decomposition of nitrate anions (202 °C), based on TGA-FTIR chromatogram data shown in Figure 6.

Reaction sequences over the above major weight losses [(i)−(iii) above] in both samples are identical, although their relative intensities are quite different (Figure 6). In particular, the peaks of dehydroxylation correspond to the beginning of nitrate decomposition in both compounds. More interestingly, the thermal event temperatures in Co^{II}-0.5 are shifted to higher temperatures, compared to those in $Co^{II,III}$-0.2. In our previous investigation, we have found that nitrate anions change their D_{3h} site symmetry to C_{2v} according to a "grafting" mechanism:[18]

$$Co^{2+} + O^{-}-NO_2 = Co^{2+}O^{-}-NO_2 \qquad (1)$$

$$Co^{2+}O^{-}-NO_2 = Co^{3+}O^{2-} + NO_2(g) \qquad (2)$$

It has been recognized that a direct attachment of an anion to Co^{2+} will further facilitate this charge-transfer process, on the basis of the symmetry change of nitrate anions (D_{3h} to C_{2v}). Following this mechanism, in principle, Co^{II}-0.5 compound should have given a lower decomposition temperature than $Co^{II,III}$-0.2 because the nitrate anions have already attached to the divalent cobalt in the compound. Furthermore, cobalt cations in Co^{II}-0.5 are all in a divalent state, which is supposed to be even more advantageous for this type of redox decomposition. Nonetheless, this is not the case, as the new observations in Figure 6 shows the opposite trend. Because decomposition of nitrate anions takes place immediately after dehydroxylation of brucite-like sheets, instead of at a fixed temperature, it is clear now that divalent cobalt cations in resultant oxides are active species for the reactions 1 and 2. Therefore, in addition to the anion configuration, the ability to form cobalt−oxides is also a key to the nitrate decomposition in these compounds.

For $Co^{II,III}$-0.2 compound, the peak at 192 °C (NO_2, Figure 6) can be assigned to the nitrate anions occupying oxygen vacant sites (naked Co^{2+}) of cobalt−oxides during the decomposition. The second peak at 270 °C could be attributed to the nitrate anions that are more difficult to change from D_{3h} to C_{2v}. Considering the electrostatic attraction between trivalent cations and intercalated anions in hydrotalcite-like structure, these nitrate ions may be strongly associated to Co^{3+} during the dehydroxylation process. As a result, higher thermal energy is required for them to diffuse to Co^{2+}. In line with this, the decomposition of nitrate ions in Co^{II}-0.5 occurs in a single-step manner at 202 °C, which includes the majority of ions in both C_{2v} and D_{3h} symmetries (Figure 4). A lasting tail after the main peak can be similarly explained as an increase in trivalent sites, that is, an increase in difficulty for D_{3h} ions to move to a

(31) Yun, S. K.; Pinnavaia, T. J. *Chem. Mater.* **1995**, *7*, 348.

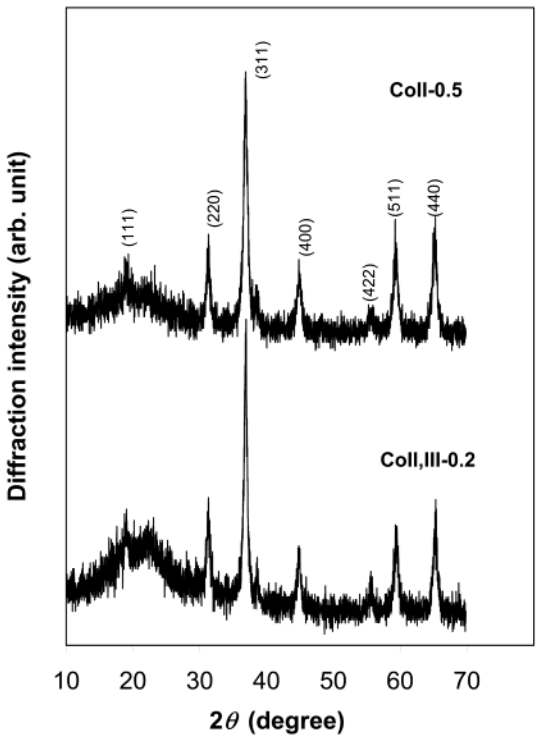

Figure 7. XRD patterns of decomposed $Co^{II,III}$-0.2 and Co^{II}-0.5 compounds. The two samples were heated from room temperature to 400 °C in nitrogen in a TGA furnace (at 10 °C min^{-1}) and then brought back to room temperature in the same inert atmosphere.

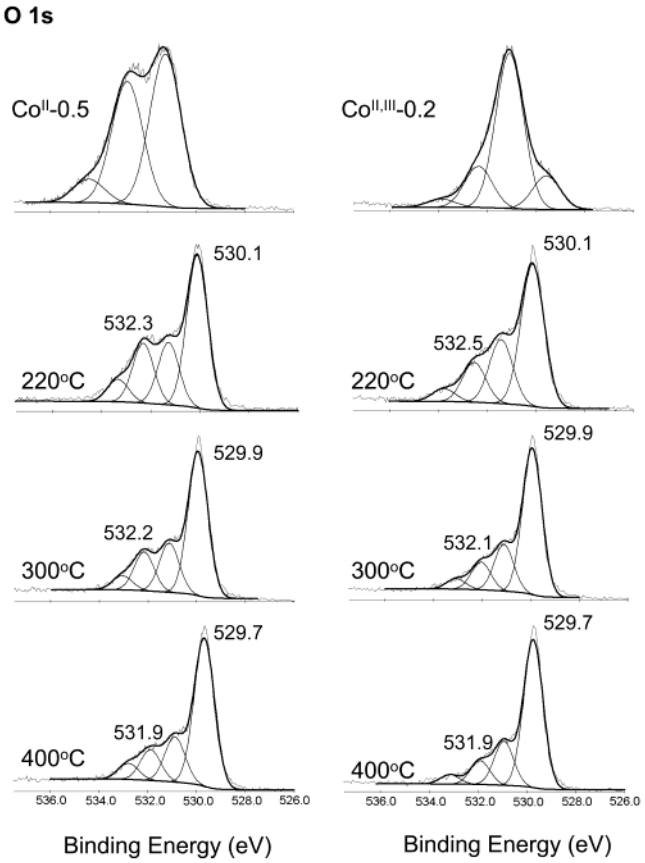

Figure 8. O 1s photoelectron spectra of $Co^{II,III}$-0.2 and Co^{II}-0.5 compounds as well as their respective samples heated over the temperature range of 220−400 °C.

divalent site. Nonetheless, despite higher nitrate content in Co^{II}-0.5, nitrate decomposition (ca. 250 °C) is still completed earlier than that in $Co^{II,III}$-0.2 (ca. 270 °C); this observation clearly supports the "direct attachment model".[18] Since the redox reactions take place between divalent cobalt cations and nitrate anions, final decomposed products for $Co^{II,III}$-0.2 and Co^{II}-0.5 are all in Co_3O_4 spinel (XRD, Figure 7; XPS, Figure 10). Due to more nitrate ions (oxidant) and more direct contact between the redox reactants, the reactions are more complete in Co^{II}-0.5, as indicated by the TGA (Figure 5 and Table 1) and TGA-FTIR (Figure 6) results. Finer Co_3O_4 crystallites (Table 1) from Co^{II}-0.5 can be attributed to the early decomposition of nitrate ions and thus low-temperature formation of crystallites.

It should be mentioned that the amount of interlayer carbonate anions in the two precursor compounds is very low, although the CO_2 absorbance in Figure 6 is high (due to high sensitivity in IR detection). In general, the decomposition of this anion shows no direct links with the nitrate, but has some connections with the dehydroxylation process, especially in the $Co^{II,III}$-0.2 case. Although there are variations in CO_2 absorbance, the peak and band positions of the two compounds are quite similar, which reflects that carbonate decomposition is merely a normal thermal process (i.e., without additional redox reactions involved), and the variations exhibited are the combination of overall layered structure stability and CO_2 adsorption selectivity on the resultant metal−oxides.[32−34] In view of its small concentration and nonoxidative nature, further elaborations on the peak assignment of CO_2 will not be made.

Surface Analysis of Decomposed Products. In Figure 8, there are four O 1s subpeaks resolved for different surface oxygen species in pristine $Co^{II,III}$-0.2. The main peak with a BE of 531.1 eV can be assigned to the hydroxyl oxygen of brucite-like layers, the peak at 532.4 eV is assigned to the oxygen of nitrate anions, and the small peak at the highest BE of 533.9 eV is assigned to the oxygen in water molecules.[35,36] The remaining O 1s peak at the lowest BE (529.6 eV), which is commonly known as the oxygen ions (O^{2-}) of metal−oxides,[35,36] could be attributed to a small degree of dehydroxylation on the topmost sample surface upon drying. The O 1s spectrum of as-prepared Co^{II}-0.5 compound can be deconvoluted into three subpeaks at BEs of 531.3 eV (hydroxyl group), 532.9 eV (nitrate group), and 534.4 eV (water), respectively.[36] Because the last peak at 534.4 eV is about 0.5 eV higher than 533.9 eV, it is believed that these water molecules on the surface of Co^{II}-0.5 are chemically adsorbed in a metal

(32) Tsuji, M.; Mao, G.; Yoshida, T.; Tamaura, Y. *J. Mater. Res.* **1993**, *8*, 1137.
(33) Pesic, L.; Salipurovic, S.; Markovic, V.; Vucelic, D.; Kagunya, W.; Jones, W. *J. Mater. Chem.* **1992**, *2*, 1069.
(34) Bellotto, M.; Rebours, B.; Clause, O.; Lynch, J.; Bazin, D.; Elkaim, E. *J. Phys. Chem.* **1996**, *100*, 8542.
(35) Zeng, H. C.; Lin, J.; Teo, W. K.; Wu, J. C.; Tan, K. L. *J. Mater. Res.* **1995**, *10*, 3096.
(36) Moulder, J. F.; Stickle, W. F.; Sobol, P. E.; Bomben, K. D. *Handbook of X-ray photoelectron spectroscopy: a reference book of standard spectra for identification and interpretation of XPS data;* Chastain, J., Ed.; Perkin-Elmer Corporation, Physical Electronics Division (Imprint): Eden Prairie, MN, 1992.

Table 2. Results of N 1s and Co 2p Spectrum Analyses (see Figures 9 and 10)

sample	N 1s BE (eV)	atomic ratio[a]	fwhm (eV)	assignment
$Co^{II,III}$-0.2	406.4	0.17	1.4	interlayer NO_3^- (D_{3h})
220 °C	406.8	0.06	1.8	surface NO_3^-
300 °C	406.7	0.01	1.9	surface NO_3^-
400 °C	−	−		−
Co^{II}-0.5	406.8	0.28	1.4	surface NO_3^-
	408.1	0.09	1.4	interlayer NO_3^- (C_{2v})
	409.5	0.04	1.4	interlayer NO_3^- (D_{3h})
220 °C	406.8	0.10	1.4	surface NO_3^-
300 °C	406.8	0.05	1.2	surface NO_3^-
400 °C	406.7	0.07	1.8	surface NO_3^-

sample	peak 1[b] (eV)	surface species	peak 2[b] (eV)	surface species	fwhm (eV)	ΔBE[d] (eV)
$Co^{II,III}$-0.2	780.6 (0.78)[c]	Co−OH	783.3 (0.22)[c]	Co−NO_3	2.6	15.5
220 °C	780.4 (0.78)	Co_3O_4	782.5 (0.22)	CoO	2.2	15.0
300 °C	780.1 (0.77)	Co_3O_4	782.3 (0.23)	CoO	2.2	15.0
400 °C	779.9 (0.74)	Co_3O_4	781.9 (0.26)	CoO	2.1	15.1
Co^{II}-0.5	781.2 (0.70)[c]	Co−OH	783.4 (0.30)[c]	Co−NO_3	2.7	15.9
220 °C	780.3 (0.74)	Co_3O_4	782.3 (0.26)	CoO	2.2	15.1
300 °C	780.1 (0.75)	Co_3O_4	782.2 (0.25)	CoO	2.1	15.1
400 °C	779.8 (0.72)	Co_3O_4	781.7 (0.28)	CoO	2.0	15.1

[a] Relative atomic ratio of nitrogen to cobalt. [b] BEs of Co $2p_{3/2}$ photoelectrons. [c] Peak area fraction in the total sum of peaks 1 and 2. [d] Separation between Co $2p_{1/2}$ and Co $2p_{3/2}$ ($\Delta BE = BE_{peak3} - BE_{peak1}$).

site (which acts as Lewis acid attracting the lone pair electrons of H_2O)[37] considering a large number of hydroxyl vacancies in this compound. For calcined samples, the O 1s spectra can be resolved well into four subpeaks, as suggested by the overall peak shape and width. Owing to the thermal treatment, fwhm's have been narrowed drastically, reflecting a more ordered surface structure in these samples. At 220 °C (Figures 5 and 6), both $Co^{II,III}$-0.2 and Co^{II}-0.5 have undergone dehydroxylation and resulted in cobalt−oxides. In this agreement, the oxide oxygen peaks at 530.1−529.7 eV increase significantly after this temperature. The remaining three subpeaks are assigned to surface hydroxyl groups (2nd peaks), nitrate anions (3rd peaks), and water (4th peaks), respectively, noting that the third peaks at 531.9−532.5 eV for Co^{II}-0.5 is higher than those of $Co^{II,III}$-0.2 because of a higher nitrate content.

In Figure 9, the N 1s peak of $Co^{II,III}$-0.2 at 406.4 eV can be assigned to intercalated nitrate anions in interlayer space, noting that this peak is shifted to 406.8 eV in the heated samples (listed in Table 2). This can be attributed to a decomposition−re-adsorption process at this temperature range (220−300 °C):

$$NO_3^-(\text{interlayer}) \rightarrow NO_2(\text{gas}) \rightarrow NO_3^-(\text{surface}) \quad (3)$$

In Co^{II}-0.5, on the other hand, there are three well-resolved N 1s subpeaks. Surface-adsorbed nitrate ions at BE = 406.8 eV is resulted from liquid−solid interfacial adsorption, as a large amount of $NaNO_3$ was used in the synthesis. According to the relative FTIR absorption intensities (Figure 2) and XPS peak areas, N 1s BEs at 408.1 and 409.5 eV are assigned respectively to model I and model II (Figure 4). Because nitrate anions of Co^{II}-0.5 are directly "grafted" into the brucite-like sheets,[23−25] a more intimate interaction between the nitrate and cobalt is anticipated in this compound, which is indeed reflected by the positive shifts of N 1s

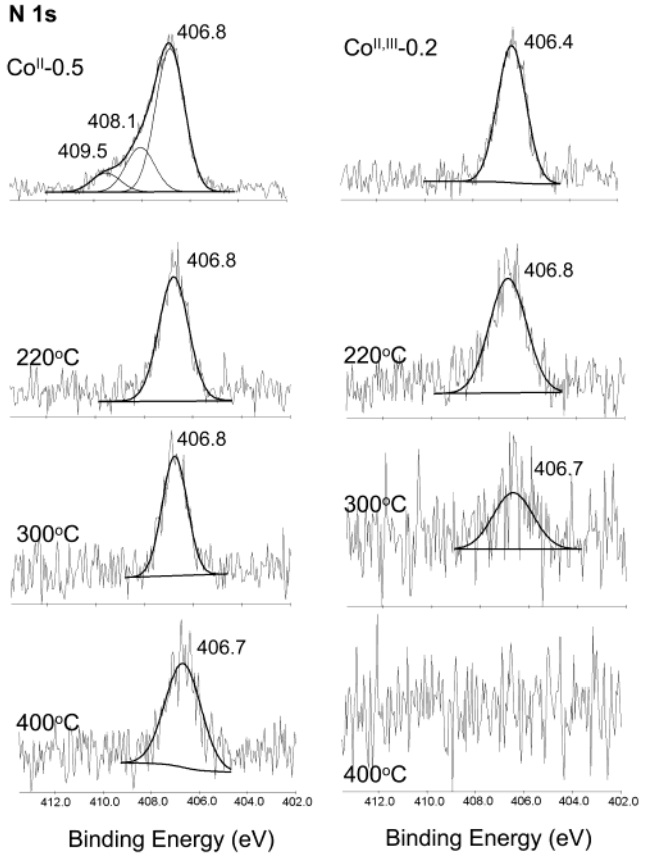

Figure 9. N 1s photoelectron spectra of $Co^{II,III}$-0.2 and Co^{II}-0.5 compounds as well as their respective samples heated over the temperature range of 220−400 °C.

owing to an overall reduction of electron density of nitrate ions. More effective electron-density lowering in model II is expected because of more delocalization of charge with D_{3h} symmetry. For Co^{II}-0.5 heated at 220−400 °C, N 1s spectra show only one peak at 406.8 eV. Once again, surface-adsorbed nitrate ions produced in the same way as reaction 3 are found. Since more nitrate ions are decomposed in this compound, more

(37) Joesph, Y.; Ranke, W.; Weiss, W. *J. Phys. Chem. B* **2000**, *104*, 3224.

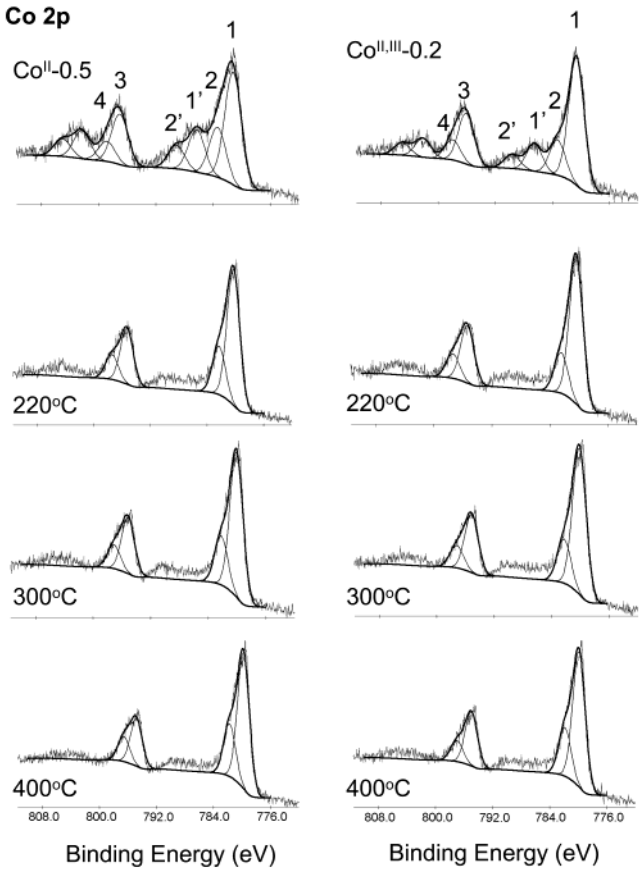

Figure 10. Co $2p_{3/2}$ and Co $2p_{1/2}$ photoelectron spectra of $Co^{II,III}$-0.2 and Co^{II}-0.5 compounds as well as their respective samples heated over the temperature range of 220−400 °C.

back-adsorbed NO_2 is expected; nitrate anions can still be detected on a 400 °C heated sample.

Co 2p photoelectrons have also been investigated to probe surface metal species upon compound decompositions. As reported in Figure 10 and Table 2, all spectra show two well-separated branches of $2p_{3/2}$ (peaks 1 and 2) and $2p_{1/2}$ (peaks 3 and 4). In $Co^{II,III}$-0.2, the peaks at 780.6 and 783.3 eV can be assigned respectively to the cobalt cations in hydroxyl octahedra and in association with nitrate anions.[10] Similarly, the peaks at 781.2 and 783.4 eV in Co^{II}-0.5 are ascribed to cobalt ions in the same respective local environments, noting that there is an increase in BE of the first peak in this compound (781.2 vs 780.6 eV) due to the modification of the hydroxyl sublattice with nitrate anions. Compared to those of $Co^{II,III}$-0.2, intensities of shake-up satellites at higher BEs (peaks 1′ and 2′) of Co^{II}-0.5 are higher, in good agreement with that expected for this high-spin compound (all cobalt ions are in divalent state). As detailed in Table 2, Co $2p_{3/2}$ BE peaks 1 and 2 are moved monotonically toward 779.9 and 781.9 eV for surface Co_3O_4 and CoO,[38−40] when these two samples are heated at 220−400 °C in nitrogen. It has been well-known that there is a chemical equilibrium between Co_3O_4 and CoO surface phases upon heating and cooling processes,[38−40] although Co_3O_4 is detected as the only bulk phase by XRD (Figure 7). The surface Co_3O_4 (peak 1) is clearly predominant, indicated by an area ratio change (Table 2) and an intensity reduction of shake-up satellites in the heated samples. BE separations between $2p_{3/2}$ and $2p_{1/2}$ branches (spin−orbit splitting) also indicate the formation of CoO−Co_3O_4 surface phases upon the self-redox decompositions of both compounds.[39−42]

Conclusions

In summary, cobalt−hydroxide−nitrates can be prepared with variable redox reagent anion contents and packing arrangements (i.e., with or without direct contact between the reductant and oxidant and having different site symmetries for nitrate anions) in their lamellar structures. Although details of decomposition are varied, reaction sequences in the two studied compounds are identical: decomposition of carbonate anions; dehydroxylation of brucite-like layers; and decomposition of nitrate anions. In addition to the "direct attachment mechanism", it is clear now that divalent cations in resulting cobalt−oxides (rather than in hydroxyl octahedra) are the active reductant for the redox reactions. Consistent with the variations in chemical and structural natures in the two compounds, the as-prepared hydrotalcite-like compound shows a higher degree of difficulty in decomposing nitrate anions, owing to the lack of C_{2v} site symmetry and adjacent divalent cations. Due to differences in the storage capacities of reagents, reaction extents of the two compounds are also different, although their final decomposed products are similar (nanophase Co_3O_4 formed at 400 °C with size in the range of 12−15 nm). Surface compositional investigation also reveals that local chemical environments for the intercalated anions and central cations of the brucite-like sheets are indeed different for the compounds with or without modification of hydroxyl sublattice. These variations are in good accordance with the actual redox reactivity observed in the decomposition processes.

Acknowledgment. The authors gratefully acknowledge research funding (R-279-000-064-112 and A/C50384) co-supported by the Ministry of Education and the National Science and Technology Board, Singapore.

CM021732O

(38) Milton, D. B.; Walton, J.; Thompson, G. E. *Surf. Interface Anal.* **1993**, *20*, 36.
(39) Oku, M.; Sato, Y. *Appl. Surf. Sci.* **1992**, *55*, 37.
(40) Zeng, H. C.; Lin, J.; Tan, K. L. *J. Mater. Res.* **1995**, *10*, 3096.
(41) Kim, K. S. *Phys. Rev. B* **1975**, *11*, 2178.
(42) Chuang, T. J.; Brundle, C. R.; Rice, D. W. *Surf. Sci.* **1976**, *59*, 413.